BC Hydro Ground Motion Prediction Equations for Subduction Earthquakes

Norman Abrahamson,[a] M.EERI, **Nicholas Gregor,**[b] M.EERI, **and Kofi Addo,**[c] M.EERI

An updated ground motion prediction equation (GMPE) for the horizontal component response spectral values from subduction zone earthquakes is developed using a global data set that includes 2,590 recordings from 63 slab earthquakes ($5.0 \leq \mathbf{M} \leq 7.9$) and 953 recordings from 43 interface earthquakes ($6.0 \leq \mathbf{M} \leq 8.4$) at distances up to 300 km. The empirical data constrain the moment magnitude scaling up to **M**8.0. For $\mathbf{M} > 8.0$, a break in magnitude scaling is included in the model based on the magnitude scaling found in numerical simulations for interface earthquakes in Cascadia. The focal depth scaling of the short-period spectral values are strong for slab earthquakes, but it is not seen for interface events. The distance scaling is different for sites located in the forearc and backarc regions, with much steeper attenuation for backarc sites. The site is classified by V_{S30} with constrained nonlinear site amplification effects. [DOI: 10.1193/051712EQS188MR]

INTRODUCTION

In 2007, BC Hydro, the major dam owner in British Columbia, Canada, began a major update of the seismic hazard assessment of their dam sites. One key issue was the ground motions from large subduction zone earthquakes on the Cascadia subduction zone. The ground motion prediction equations (GMPEs) for subduction zone earthquakes available at the time showed a large range in the median ground motion values and, in some cases, had very large aleatory variability (BC Hydro 2012, Douglas 2010) when compared to recently developed crustal ground motion models (Abrahamson et al. 2008). Rather than using the available GMPEs, it was decided to develop a suite of new GMPEs for subduction zone earthquakes, taking advantage of the significant increase in available subduction zone ground motion recordings not included in current GMPE data sets. The new subduction GMPE developed as part of that study is described in significant detail in BC Hydro (2012), including a comprehensive set of residual plots and comparisons with other subduction GMPE models. An overview and summary of the BC Hydro (2012) subduction GMPE is presented in this paper.

DATA SET

A key component of the development of a new global empirical prediction model for subduction zone earthquakes is the compilation of a global data set of empirical

[a] University of California, Berkeley, CA 94720
[b] Consultant, Oakland, CA 94612
[c] BC Hydro, Burnaby, BC, Canada

Earthquake Spectra, Volume 32, No. 1, pages 23–44, February 2016;

strong-motion data. Several studies (e.g., Crouse et al. 1988, Crouse 1991, Youngs et al. 1997, Atkinson and Boore 2003, 2008, Zhao et al. 2006, Lin and Lee 2008) developed empirically based subduction zone ground motion prediction models based on different data sets of subduction zone strong-motion recordings. For the BC Hydro (2012) study, the initial ground motion data set was taken from the Atkinson and Boore (2003, 2008) data set, which included a compilation of earlier data sets of Crouse et al. (1988), Crouse (1991), and Youngs et al. (1997). Additional subduction ground motion data were obtained for events in Japan (Zhao 2008), Taiwan (Cheng 2008), South and Central America (Pacific Engineering 2008) and Mexico (Macias-Carrasco 2008).

The entire data set consists of 9,946 ground motion record pairs (two horizontal components) from 292 subduction zone earthquakes. A total of 3,557 record pairs are from 163 interface events and 6,389 record pairs are from 129 intraslab events. In compiling the data set, available metadata, acceleration response spectra and processed time histories were obtained when available. For some older earthquakes in the data set, the acceleration time histories could not be obtained and ground motion values were only available for PGA and 5% damped response spectra at six spectral periods: 0.1, 0.2, 0.4, 1.0, 2.0, and 3.0 seconds.

For earthquakes with available time histories, the 5% damped spectral-acceleration response spectra were computed for a suite of 19 spectral periods between 0.01 s and 5.0 s. The useable period range was determined for each recording based on the corner frequencies of the filters used in the processing: the minimum usable frequency was set at 1.2 times the corner frequency of the high-pass filter (Chiou et al. 2008). For all of the computed response spectra, except for the Taiwan data, the geometric mean of the two horizontal components was computed. The older legacy data was assumed to be the geometric mean of the two horizontal components. The spectral acceleration values for the Taiwan data were provided by Cheng (2008) and are based on GMRotI50 as defined in Boore et al. (2006). Beyer and Bommer (2006) showed that the average difference between GMRotI50 and the geometric mean of the two horizontal components is negligible; thus, we do not expect the different definitions of ground motion between the two data sets to have a significant impact on the regression.

METADATA

In compiling the data set of subduction ground motions, metadata were adopted from the source of each contributing data set. These metadata typically consist of the following parameters: moment magnitude, event type (either interface or intraslab), epicentral location and depth, aftershock/foreshock identification, station location, site classification, forearc or backarc classification, distance metrics (rupture distance and hypocentral distance), and the shear wave velocity over the top 30 m (V_{S30}).

Magnitude, Location, Depth, and Interface/Intraslab Classification

A preliminary analysis of the composite data set found that there were possible errors in the classification of interface events as intraslab events and vice versa. Therefore, the event classification was re-evaluated based on focal depth location, subduction zone tectonics, and event focal mechanism. This simplified re-examination is similar to the more detailed

approach described in Garcia et al. (2012). For events with hypocentral depths deeper than 30 km (events with depths less than 30 km were not re-examined), the ISC seismicity catalog (ISC 2014) was used to better determine magnitudes, locations, and hypocentral depths.

For magnitude, a preference for the estimated moment magnitude was given to the Global Central Moment Tensor (GCMT) catalog solution (Ekström et al. 2012). In cases for which there was no GCMT solution but for which a regional CMT solution was available, the magnitude from the regional CMT solution was adopted. In the analysis of events with depths greater than 30 km, none of the earthquake magnitudes showed a significant change from the values given in the source data sets.

Several epicentral locations (i.e., latitude and longitude) and, more important, depth estimates appeared to be in error or were missing for some earthquakes in the data set. In searching the ISC catalog, missing or erroneous hypocentral locations were replaced with ISC locations or the GCMT solution location when available. For depth estimates, any hypocentral depth determined from the pP seismic phase was given preference over other hypocentral depth estimates.

As part of the refinement of hypocentral depth values from the ISC catalog, a review of the event classification type (i.e., interface or intraslab) was performed. Given the preferred ISC hypocentral depths, GCMT solution, and/or first motion fault plane solutions, the event classification was either confirmed or changed to be consistent with the updated metadata information. This review resulted in a total of nine events classified as intraslab beingreclassified as interface. The deepest of these nine events had a hypocentral depth of 53.0 km.

Site Classification and V_{S30}

An estimate of V_{S30} was developed for each station in the data set. In some cases, measured V_{S30} values were available, but for most stations correlations between site classifications and average V_{S30} values were used to estimate V_{S30}.

For the recently obtained data from Japan (Zhao 2008), Central and South America (Pacific Engineering and Analysis 2008), Mexico (Macias-Carrasco 2008), and Taiwan (Cheng 2008), estimates of V_{S30} values were submitted along with each data set. For older data sets (e.g., Youngs et al. 1997, Atkinson and Boore 2003, 2008), the sites were classified into broad categories. For the Youngs et al. (1997) data set, the site categories were based on the Geomatrix third letter code (see Chiou et al. 2008); for the Atkinson and Boore (2003, 2008) data set, the site categories were based on the NEHRP classification scheme. Correlations between the Geomatrix third letter code, the NEHRP site classifications (Chiou et al., 2008), and average V_{S30} values are provided in Table A1 (online Appendix).

Forearc/Backarc Station Classification

Based onpreliminary analysis of the subduction data set, the classification of stations located in the forearc region (i.e., between the subduction trench axis and the axis of volcanic fronts) as opposed to the backarc region indicated a possible variation in the rate and characteristics of ground motion attenuation between these two regions. Stations from Japan, Cascadia (see BC Hydro 2012 for classification boundaries for the sites used in the PSHA study), and Taiwan were all classified as located in the forearc or backarc region

based on the relative locations of observed volcanic fronts for each subduction zone region. It should be noted that almost all of the backarc data in the database are from Japanese stations and the differences in backarc attenuation may be a regional effect rather than a global backarc difference.

Distance Measure

Each of the contributing data sets reported a single distance measure for each record. Unfortunately, the definition of this distance measure was not contained in associated documentation for all of the data sets, especially for the older cases. Distances were adopted from the contributing data sets without a re-evaluation. For the older subduction zone earthquakes contained in the Youngs et al. (1997) data set, the reported distance values were hypocentral distances for all intraslab events and for interface events of magnitudes less than approximately 7.5. For interface events with magnitudes larger than approximately 7.5, the distances reported in the Youngs et al. (1997) data set are given as rupture distances (Youngs, *pers. comm*., 2011). For deep and relatively small-magnitude intraslab events, the difference between a rupture distance and a hypocentral distance would not be significant. For shallow and large-magnitude interface events, the difference in rupture distance versus hypocentral distance could be significant.

SELECTION OF FINAL DATA SET

For data whose reliability or applicability was questionable, the decision was to remove them rather than try to resolve the problem with data. For example, data that were clear outliers (e.g., off by factors of 100 or more) were simply removed and no attempt was made to identify and correct the problem. An example of this data applicability issue is the 1992 Cape Mendocino earthquake (**M**7.0), which was not clearly an interface or a crustal event and so was removed from the data set used for this study.

In addition, since the focus for the interface events was on large-magnitude interface earthquakes and moderate- to large- magnitude events for intraslab events based on the controlling events for the BC Hydro facilities (BC Hydro 2012), two additional constraints were applied to remove the smaller-magnitude events: (1) exclusion of interface events with magnitudes less than 6.0 and (2) exclusion of intraslab events with magnitudes less than 5.0

Following the completion of the subduction data set, two large interface earthquakes occurred: 2010 Chile (**M**8.8) and 2011 Tohoku, Japan (**M**9.0). These two earthquakes provided the first large sets of ground motions from interface earthquakes above **M**8.7. The data were used to check and revise the large-magnitude scaling of the model, as described later.

Data Censoring

For the regression analysis, the data set should be unbiased. At large distances, one common source of bias in ground motion data results from trigger thresholds. At these distances, ground motions that are above average may exceed the trigger threshold, but the ground motions that are below average may not. This results in the recorded ground motions being skewed to higher ground motions. If these biased data are used in the regression,

the slope of the distance attenuation will be too gentle (i.e., flatter attenuation). The distance at which the truncation of the ground motion distribution occurs depends on magnitude, with smaller-magnitude events being affected at shorter distances than large-magnitude earthquakes. To avoid this problem of data censoring, magnitude-dependent distance limits for both interface and intraslab events are applied to the ground motion data set based on the PGA (Figure A1) in the online Appendix. The full details of this censoring approach and results are presented in BC Hydro (2012) report. The resulting data set, including the earthquake metadata and the number of recordings from each event, is listed in Table A2 in the online Appendix. In addition, the summary statistics of the number of recordings from specific regions is given in Table A3 in the online Appendix. The resulting data set (i.e., 953 recordings from 43 interface events and 2,590 recordings from 63 slab events) is shown in Figure 1, plotted versus rupture distance for the interface events and hypocentral distance for the intraslab events.

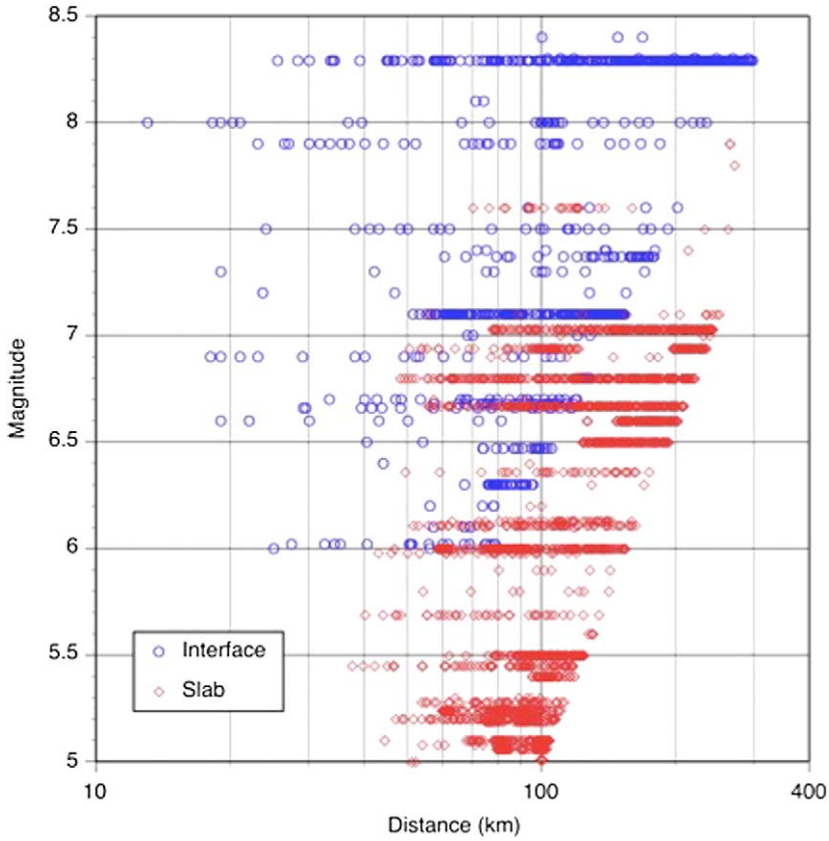

Figure 1. Distribution of magnitude and distance (interface events are plotted versus rupture distance; intraslab events, versus hypocentral distance) in the final data set used to develop the GMPE, prior to the 2010 Maule, Chile, and 2011 Tohoku, Japan, earthquakes.

MODEL FORM DEVELOPMENT

BASE MODEL FUNCTIONAL FORM

A preliminary evaluation of the data showed that magnitude scaling over the range **M**5.0–**M**7.0 for slab events is similar to magnitude scaling for **M**6.0–**M**8.0 interface earthquakes (with a constant offset). Therefore, a common magnitude scaling was used. An issue is where a break in the magnitude scaling at high magnitudes (**M** > 8.0) occurs that is not well represented in the empirical data.

The magnitude scaling for large events was evaluated using numerical simulations. Gregor et al. (2002) and Atkinson and Macias (2009) both used finite-fault simulations to estimate ground motions from large interface events on the Cascadia subduction zone. The PGA scaling from these two simulations is shown in Figure 2 along with the preliminary magnitude scaling from the empirical data grouped in half-magnitude unit bins and corrected for similar rock site conditions and a distance of 100 km. Both sets of simulations show

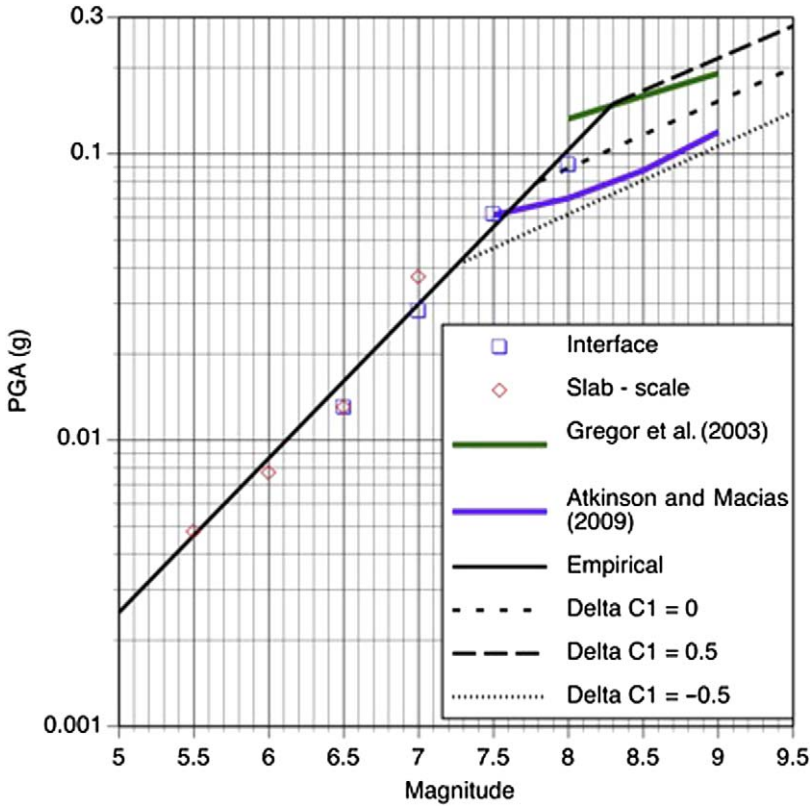

Figure 2. PGA magnitude scaling at a distance of 100 km adjusted for similar rock site conditions. The slab ground motions have been shifted down by a constant factor to agree with the interface ground motions for **M**6.5.

weaker magnitude scaling for large ($\mathbf{M} > 8.0$) magnitudes as compared to the magnitude scaling obtained from the empirical data at smaller magnitudes. To account for the break in magnitude scaling seen in the simulations, the functional form of the ground motion model is constrained to have a break in the magnitude scaling near **M**7.8.

There are two commonly used functional forms of the base model for PGA that capture the saturation at short distances: a magnitude-dependent slope and a magnitude-dependent fictitious depth. The Gregor et al. (2002) model, based on finite-fault simulations, uses the magnitude-dependent fictitious-depth functional form. To allow the empirical data to constrain scaling, a combination of both models is used with the magnitude dependence of the fictitious depth constrained (i.e., fixed coefficient) by the numerical simulations and the magnitude-dependent slope estimated from the empirical data, given the magnitude-dependent fictitious depth. The geometrical spreading terms (see Equation 1) are highly correlated with the saturation terms and cannot all be determined from the data. Therefore, one of the values had to be constrained. We chose to constrain the fictitious-depth term to 10 km, but this value is not critical: if a different value were selected (5 km or 15 km), the other terms would simply adjust.

HYPOCENTRAL-DEPTH SCALING

An initial regression using the complete data set was conducted without hypocentral-depth dependence, and initial residuals were computed as a function of hypocentral depth (BC Hydro 2012). For interface earthquakes, the interevent residuals did not visually show a trend with hypocentral depth; however, for intraslab earthquakes, there was strong trend with depth (see Figure A2 in the online Appendix). Based on this analysis, the functional model used in the regression included a hypocentral-depth term for the intraslab events but not for the interface events. A depth limit of 120 km is recommended for intraslab events when applying the model.

BACKARC ATTENUATION

An initial regression was conducted without a difference between forearc and backarc sites. The distance dependence of the intraevent residuals are shown in Figures A3 and A4 in the online Appendix for interface and intraslab earthquakes, respectively. For both earthquake types, there is a trend in the distance dependence of the residuals, with backarc sites showing a negative slope that implies steeper attenuation. To account for this difference, separate distance attenuation is included for backarc sites with separate slopes for interface and intraslab earthquakes.

SITE AMPLIFICATION

The subduction data are not adequate to constrain nonlinear site amplification. Nonlinear site effects should apply to subduction earthquakes in the same way they apply to crustal earthquakes. Therefore, the amplification nonlinearity is constrained to be consistent with the Peninsula Range model (Walling et al. 2008, with minor rounding of the reference V_{S30} to 1,000 m/s from 1,100 m/s) used for two of the NGA relations (Abrahamson and Silva 2008, Campbell and Bozorgnia 2008).

REGRESSION ANALYSIS

FUNCTIONAL FORM OF MODEL

From the initial evaluations described earlier and presented in greater detail in BC Hydro (2012), the following functional form was used for the regression analysis:

$$\ln(Sa_{interface}) = \theta_1 + \theta_4 \Delta C_1 + (\theta_2 + \theta_3(M - 7.8)) \ln(R_{rup} + C_4 \exp(\theta_9(M - 6))) + \theta_6 R_{rup} + f_{mag}(M) + f_{FABA}(R_{rup}) + f_{site}(PGA_{1100}, V_{S30}) \quad (1a)$$

$$\ln(Sa_{slab}) = \theta_1 + \theta_4 \Delta C_1 + (\theta_2 + \theta_{14} F_{event} + \theta_3(M - 7.8)) \ln(R_{hypo} + C_4 \exp(\theta_9(M - 6))) + \theta_6 R_{hypo} + \theta_{10} F_{event} + f_{mag}(M) + f_{depth}(Z_h) + f_{FABA}(R_{hypo}) + f_{site}(PGA_{1100,V_{S30}}) \quad (1b)$$

where

Sa = spectral acceleration in units of g

M = moment magnitude

Z_h = hypocentral depth (km)

$$F_{event} = \begin{cases} 0 & Interface\ Events \\ 1 & Intraslab\ Events \end{cases}$$

$$F_{FABA} = \begin{cases} 0 & Forearc\ or\ Unknown\ Sites \\ 1 & Backarc\ Sites \end{cases}$$

The model for magnitude scaling is given by

$$f_{mag}(M) = \begin{cases} \theta_4(M - (C_1 + \Delta C_1)) + \theta_{13}(10 - M)^2 & for\ M \le C_1 + \Delta C_1 \\ \theta_5(M - (C_1 + \Delta C_1)) + \theta_{13}(10 - M)^2 & for\ M > C_1 + \Delta C_1 \end{cases} \quad (2)$$

where $C_1 = 7.8$.

Values of ΔC_1 capture the epistemic uncertainty surrounding the break in magnitude scaling. Initially, ΔC_1 was defined as 0.0; however, based on analysis of two recent large interface earthquakes presented later in this paper, period-dependent variations in this parameter are recommended.

The model for depth scaling is given by

$$f_{depth}(Z_h) = \theta_{11}(\min(Z_h, 120) - 60) F_{event} \quad (3)$$

The model for forearc/backarc scaling is given by

$$f_{FABA}(R) = \begin{cases} \left[\theta_7 + \theta_8 Ln\left(\frac{\max(R_{hypo},85)}{40}\right)\right] F_{FABA} & for\ F\ event = 1 \\ \left[\theta_{15} + \theta_{16} Ln\left(\frac{\max(R_{rup},100)}{40}\right)\right] F_{FABA} & for\ F\ event = 0 \end{cases} \quad (4)$$

The model for site response scaling is given by

$$f_{site}(PGA_{1000}, V_{S30}) = \begin{cases} \theta_{12} Ln\left(\frac{V_S^*}{V_{lin}}\right) - bLn(PGA_{1000} + c) + & for\ V_{S30} < V_{lin} \\ \quad bLn\left(PGA_{1000} + c\left(\frac{V_S^*}{V_{lin}}\right)^n\right) & \\ \theta_{12} Ln\left(\frac{V_S^*}{V_{lin}}\right) + bnLn\left(\frac{V_S^*}{V_{lin}}\right) & for\ V_{S30} \geq V_{in} \end{cases} \quad (5)$$

where PGA_{1000} = Median PGA value for $V_{S30} = 1{,}000$ m/s; and

$$V_S^* = \begin{cases} 1{,}000 & for\ V_{S30} > 1{,}000 \\ V_{S30} & for\ V_{S30} \leq 1{,}000 \end{cases} \quad (6)$$

REGRESSION METHODOLOGY

The regression is based on the random-effect approach following the algorithm described in Abrahamson and Youngs (1992). This algorithm uses an iterative approach to find the maximum-likelihood solution as follows:

1. Set the interevent residuals to zero: $\eta_i = 0$.
2. Subtract the estimate of the interevent residual from the observed ground motion: $y'_{ij} = y_{ij} - \eta_i$.
3. Estimate the coefficients θ_i, fitting y'_{ij} using ordinary least squares.
4. Compute median ground motion μ_{ij} for each recording, given θ_i.
5. Given the median estimates (μ_{ij}), find ϕ (intraevent variability) and τ (interevent variability) by maximum likelihood.
6. Given ϕ and τ, estimate interevent residuals η_I

Repeat Steps 2–6 until the likelihood reaches a maximum.

The log likelihood function is given by

$$LL = \left[\sum_{i=1}^{N_{eqk}} \sum_{j=1}^{N_j} \frac{(y_{ij} - \mu_{ij})}{2\phi^2} \left((y_{ij} - \mu_{ij}) - \frac{\rho S_i}{(1 + N_{i\rho})}\right)\right] - \left[\sum_{i=1}^{N_{eqk}} \sum_{j=1}^{N_j} \ln(\phi^2 + N_i\tau^2) + \ln(\phi^2)(N_i - 1)\right] \quad (7)$$

where

$$S_i = \sum_{i=1}^{N_i} y_{ij} - \mu_{ij} \tag{8}$$

and

$$\rho = \frac{\tau^2}{\phi^2} \tag{9}$$

Given ϕ and τ, the maximum-likelihood solution for the interevent residual is given by

$$\eta_i = \frac{\tau^2 \sum_{j=1}^{N_i} y_{ij} - \mu_{ij}}{N_i \tau^2 + \phi^2} \tag{10}$$

REGRESSION RESULTS

The coefficients were estimated in a series of steps (Table 1), in which the coefficients were smoothed one or two at a time and then held fixed as the remaining unsmoothed coefficients were recomputed. This multistep procedure was implemented to produce smooth spectra. To avoid having poorly recorded earthquakes impacting the scaling for magnitude, depth, and distance, only earthquakes with five or more recordings were used until the final regression run.

In the first run, only PGA is used. The linear magnitude-scaling terms (θ_4 and θ_5) and the magnitude dependence of the distance attenuation term (θ_3) are estimated for PGA and then constrained to these values for all other periods. The period-independent coefficients are listed in Table 2.

The final two runs (7 and 8) differed in the minimum number of stations. This provided a sensitivity of the results to the large number of poorly recorded earthquakes. The differences are small (BC Hydro 2012), indicating that the median model is not strongly affected by the inclusion of poorly recorded earthquakes. The final set of smoothed model coefficients (from Run 8) are listed in Table 3.

The correlation coefficients are computed for the normalized interevent and intraevent residuals separately. For application in seismic hazard, the correlation coefficient for the total

Table 1. Iteration steps used in the regression along with fixed and smoothed coefficients

Run	Minimum Stations	Fixed coefficients	Smoothed after run
1	5	PGA only, θ_9, C_4	θ_3, θ_4, θ_5
2	5	θ_3, θ_4, θ_5, θ_9	θ_2
3	5	θ_2, θ_3, θ_4, θ_5, θ_9	θ_{14}
4	5	θ_2, θ_3, θ_4, θ_5, θ_9, θ_{14}	θ_8, θ_{16}
5	5	θ_2, θ_3, θ_4, θ_5, θ_8, θ_9, θ_{14}, θ_{16}	θ_{11}, θ_{13}
6	5	θ_2, θ_3, θ_4, θ_5, θ_8, θ_9, θ_{11}, θ_{13}, θ_{14}, θ_{16}	θ_6, θ_{10}, θ_{12}
7	5	θ_2, θ_3, θ_4, θ_5, θ_8, θ_9, θ_{10}, θ_{11}, θ_{13}, θ_{14}, θ_{16}	θ_1, θ_7, θ_{15}
8	2	θ_2, θ_3, θ_4, θ_5, θ_8, θ_9, θ_{10}, θ_{11}, θ_{12}, θ_{13}, θ_{14}, θ_{16}	θ_1, θ_7, θ_{15}

Table 2. Period-independent subduction model coefficients used in the regression analysis

Coefficient	Value over all periods
n	1.18
c	1.88
θ_3	0.1
θ_4	0.9
θ_5	0.0
θ_9	0.4
C_4	10

residual is given by combining the correlations for the intraevent (ρ_{intra}) and interevent (ρ_{inter}) terms:

$$\rho_{total\ resid}(T_0, T) = \frac{\phi^2 \rho_{intra}(T_0, T) + \tau^2 \rho_{inter}(T_0, T)}{\phi^2 + \tau^2} \tag{11}$$

where T_0 = the period of interest; T = the conditioning period; and ϕ and τ = the interevent and intraevent standard deviations.

The correlation coefficients for application to the total residual are listed in Table A4 in the online Appendix.

RESIDUALS

In this section, residuals from the regression analysis are shown as functions of all of the main independent parameters to allow an evaluation of the model. The residuals are shown for PGA and spectral periods of 0.2 s, 1.0 s, and 3.0 s. Full plots of all residuals are given in BC Hydro (2012).

INTEREVENT RESIDUALS

The interevent residuals are plotted as functions of magnitude in Figure 3a (PGA and $T = 0.2$ s) and Figure 3b ($T = 1.0$ and 3.0 s). The average interevent residuals by region computed using all distances as a function of spectral periods are shown in Figures A5a–A5d in the online Appendix. For regions in which the number of recordings is small, trends are observed in the residuals. Overall, the interevent residuals do not show a strong regional difference. The exception is the Cascadia region, for which the short-period event terms are negative. These low Cascadia event terms, which are based on the five Cascadia slab events, are considered part of the epistemic uncertainty discussed later.

INTRAEVENT RESIDUALS

The distance dependencies of the intraevent residuals are shown in Figures 4a–4b for PGA and $T = 1.0$ s spectral acceleration. The residuals are separated into the forearc and backarc stations for the interface and intraslab events. No trend with distance is seen in

Table 3. Regression coefficients for the median (g) subduction GMPE model

Period (s)	V_{lin}	b	θ_1	θ_2	θ_6	θ_7	θ_8	θ_{10}	θ_{11}	θ_{12}	θ_{13}	θ_{14}	θ_{15}	θ_{16}	ϕ	τ	σ
0.000	865.1	−1.186	4.2203	−1.350	−0.0012	1.0988	−1.42	3.12	0.0130	0.980	−0.0135	−0.40	0.9996	−1.00	0.60	0.43	0.74
0.020	865.1	−1.186	4.2203	−1.350	−0.0012	1.0988	−1.42	3.12	0.0130	0.980	−0.0135	−0.40	0.9996	−1.00	0.60	0.43	0.74
0.050	1053.5	−1.346	4.5371	−1.400	−0.0012	1.2536	−1.65	3.37	0.0130	1.288	−0.0138	−0.40	1.1030	−1.18	0.60	0.43	0.74
0.075	1085.7	−1.471	5.0733	−1.450	−0.0012	1.4175	−1.80	3.37	0.0130	1.483	−0.0142	−0.40	1.2732	−1.36	0.60	0.43	0.74
0.100	1032.5	−1.624	5.2892	−1.450	−0.0012	1.3997	−1.80	3.33	0.0130	1.613	−0.0145	−0.40	1.3042	−1.36	0.60	0.43	0.74
0.150	877.6	−1.931	5.4563	−1.450	−0.0014	1.3582	−1.69	3.25	0.0130	1.882	−0.0153	−0.40	1.2600	−1.30	0.60	0.43	0.74
0.200	748.2	−2.188	5.2684	−1.400	−0.0018	1.1648	−1.49	3.03	0.0129	2.076	−0.0162	−0.35	1.2230	−1.25	0.60	0.43	0.74
0.250	654.3	−2.381	5.0594	−1.350	−0.0023	0.9940	−1.30	2.80	0.0129	2.248	−0.0172	−0.31	1.1600	−1.17	0.60	0.43	0.74
0.300	587.1	−2.518	4.7945	−1.280	−0.0027	0.8821	−1.18	2.59	0.0128	2.348	−0.0183	−0.28	1.0500	−1.06	0.60	0.43	0.74
0.400	503.0	−2.657	4.4644	−1.180	−0.0035	0.7046	−0.98	2.20	0.0127	2.427	−0.0206	−0.23	0.8000	−0.78	0.60	0.43	0.74
0.500	456.6	−2.669	4.0181	−1.080	−0.0044	0.5799	−0.82	1.92	0.0125	2.399	−0.0231	−0.19	0.6620	−0.62	0.60	0.43	0.74
0.600	430.3	−2.599	3.6055	−0.990	−0.0050	0.5021	−0.70	1.70	0.0124	2.273	−0.0256	−0.16	0.5800	−0.50	0.60	0.43	0.74
0.750	410.5	−2.401	3.2174	−0.910	−0.0058	0.3687	−0.54	1.42	0.0120	1.993	−0.0296	−0.12	0.4800	−0.34	0.60	0.43	0.74
1.000	400.0	−1.955	2.7981	−0.850	−0.0062	0.1746	−0.34	1.10	0.0114	1.470	−0.0363	−0.07	0.3300	−0.14	0.60	0.43	0.74
1.500	400.0	−1.025	2.0123	−0.770	−0.0064	−0.0820	−0.05	0.70	0.0100	0.408	−0.0493	0.00	0.3100	0.00	0.60	0.43	0.74
2.000	400.0	−0.299	1.4128	−0.710	−0.0064	−0.2821	0.12	0.70	0.0085	−0.401	−0.0610	0.00	0.3000	0.00	0.60	0.43	0.74
2.500	400.0	0.000	0.9976	−0.670	−0.0064	−0.4108	0.25	0.70	0.0069	−0.723	−0.0711	0.00	0.3000	0.00	0.60	0.43	0.74
3.000	400.0	0.000	0.6443	−0.640	−0.0064	−0.4466	0.30	0.70	0.0054	−0.673	−0.0798	0.00	0.3000	0.00	0.60	0.43	0.74
4.000	400.0	0.000	0.0657	−0.580	−0.0064	−0.4344	0.30	0.70	0.0027	−0.627	−0.0935	0.00	0.3000	0.00	0.60	0.43	0.74
5.000	400.0	0.000	−0.4624	−0.540	−0.0064	−0.4368	0.30	0.70	0.0005	−0.596	−0.0980	0.00	0.3000	0.00	0.60	0.43	0.74
6.000	400.0	0.000	−0.9809	−0.500	−0.0064	−0.4586	0.30	0.70	−0.0013	−0.566	−0.0980	0.00	0.3000	0.00	0.60	0.43	0.74
7.500	400.0	0.000	−1.6017	−0.460	−0.0064	−0.4433	0.30	0.70	−0.0033	−0.528	−0.0980	0.00	0.3000	0.00	0.60	0.43	0.74
10.000	400.0	0.000	−2.2937	−0.400	−0.0064	−0.4828	0.30	0.70	−0.0060	−0.504	−0.0980	0.00	0.3000	0.00	0.60	0.43	0.74

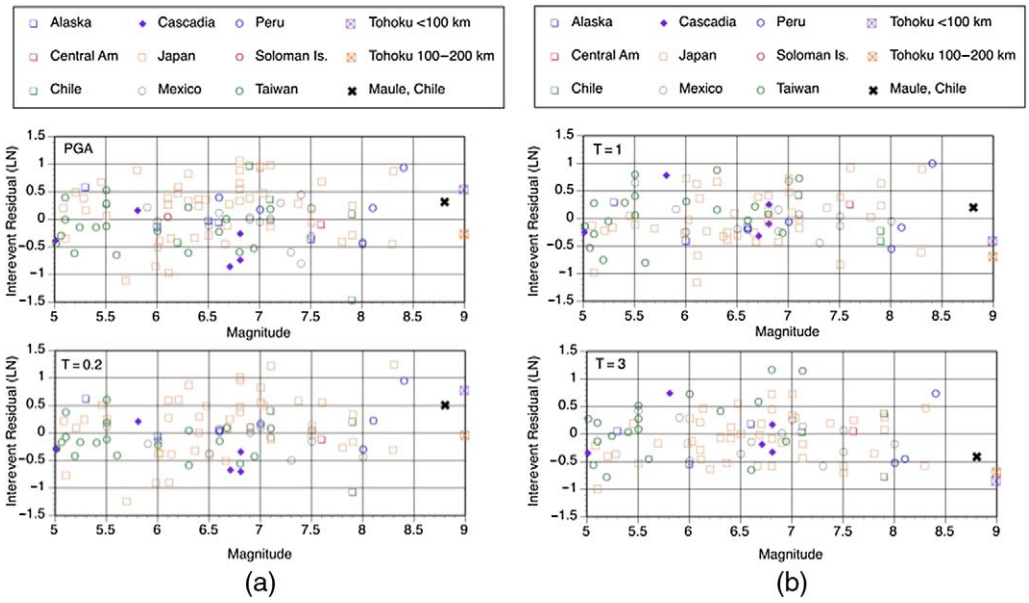

Figure 3. (a) Interevent residuals for PGA and $T = 0.2$-s spectral acceleration. The event terms from the 2010 Maule, Chile, and 2011 Tohoku, Japan, earthquakes are also shown but were not part of the data set used in the regression. (b) Interevent residuals for $T = 1.0$-s and $T = 3.0$-s spectral acceleration. The event terms from the 2010 Maule, Chile, and 2011 Tohoku, Japan, earthquakes are also shown but were not part of the data set used in the regression.

the residuals for either the backarc or the forearc stations. This indicates that the model is adequately capturing the change in the attenuation between forearc and backarc sites.

The site response model is evaluated through the V_{S30} dependence of the within-event residuals, shown in Figures 5a–5b. Overall, there are no trends in the residuals as a function of V_{S30}, indicating that the data are consistent with the commonly used form of the site amplification.

STANDARD DEVIATION

The standard deviation components were estimated for interevent and intraevent residuals. The period dependence of the interevent and intraevent standard deviations (ϕ and τ, respectively) is shown in Figure 6. A smoothed value averaged over all spectral periods is used for ϕ and τ (see Table 3). The total standard deviation is given by $\sqrt{\phi^2 + \tau^2}$. An associated single-station sigma model for the GMPE was developed and is presented in BC Hydro (2012).

COMPARISON WITH 2010 MAULE, CHILE, AND 2011 TOHOKU, JAPAN, EARTHQUAKES

After the regression analysis was completed, two large megathrust earthquakes occurred that were well recorded: the **M**8.8 2010 Maule, Chile, earthquake (Boroschek et al. 2012) and

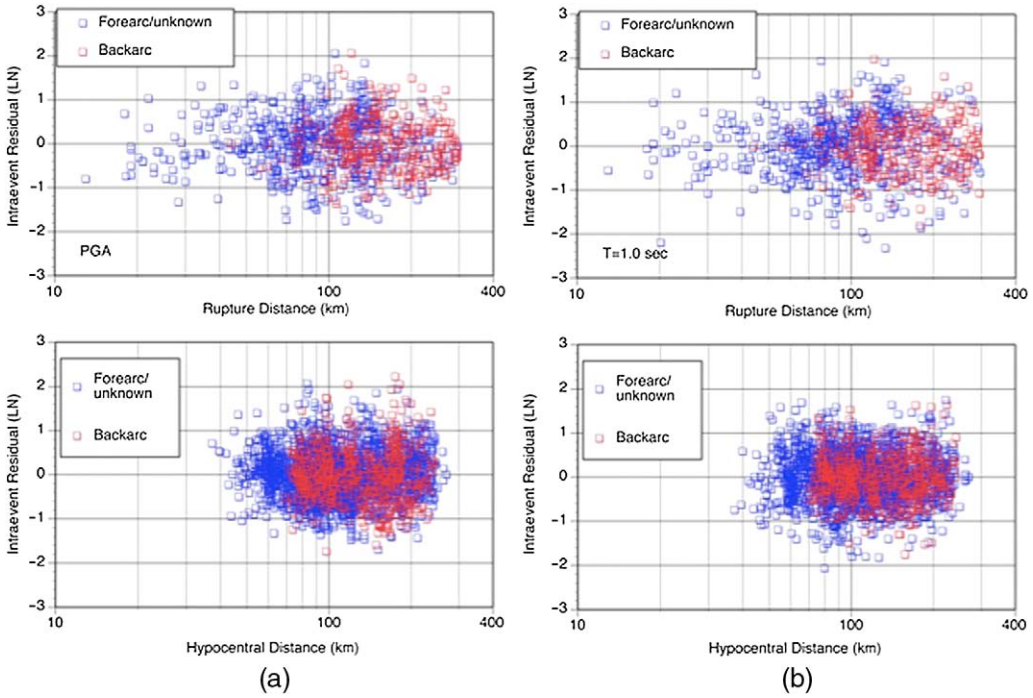

Figure 4. (a) Distance dependence of the intraevent residuals for PGA: interface earthquakes (PGA) (*top*) and slab earthquakes (PGA) (*bottom*). (b) Distance dependence of the intraevent residuals for $T = 1.0$-s spectral acceleration: interface earthquakes ($T = 1.0$ s) (*top*); slab earthquakes ($T = 1.0$ s) (*bottom*).

the **M**9.0 2011 Tohoku, Japan, earthquake (Stewart et al. 2013). Ground motions from these two earthquakes were used to evaluate the derived GMPE in the **M**9 range. The distance attenuation of the PGA and $T = 1.0$-s spectral acceleration from the 2011 Tohoku earthquake are compared to the median model predictions in Figures A6a and A6b in the online Appendix. For PGA the comparison figure indicates that the distance attenuation of short-period ground motions for forearc sites is much stronger in the 2011 data than in the GMPE, but that the distance attenuation on backarc sites is similar. For $T = 1.0$-s spectral acceleration, the distance attenuation for long periods ($T = 1.0$ s) is similar to the GMPE for both forearc and backarc sites. For the 2010 Maule, Chile, earthquake, the distance attenuation (BC Hydro 2012) is similar to the model for both short and long periods, so the steeper attenuation for short periods seen in the Tohoku earthquake is likely a region-specific effect. This regional difference for motions from Japan has also been observed for crustal events (Campbell and Bozorgnia, 2014).

The event terms represent a shift in the ground motion level and only make sense if there is not a strong distance slope to the residuals over the range of distances used to compute the event terms. The event terms from the 2010 Maule and 2011 Tohoku earthquakes are shown in Figure 7. For the Maule earthquake, a single event term from all distances is shown

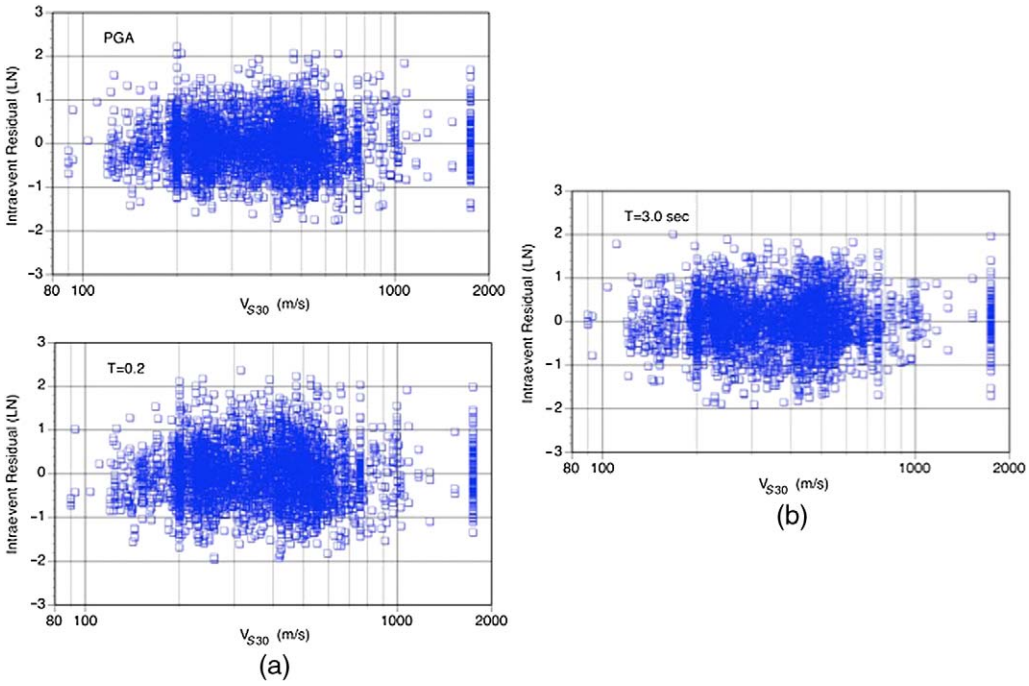

Figure 5. (a) V_{S30} dependence of the intraevent residuals for PGA (*top*) and for $T = 0.2$-s spectral acceleration (*bottom*). (b) V_{S30} dependence of the intraevent residuals for $T = 1.0$-s spectral acceleration (*top*) and for $T = 3$-s spectral acceleration (*bottom*).

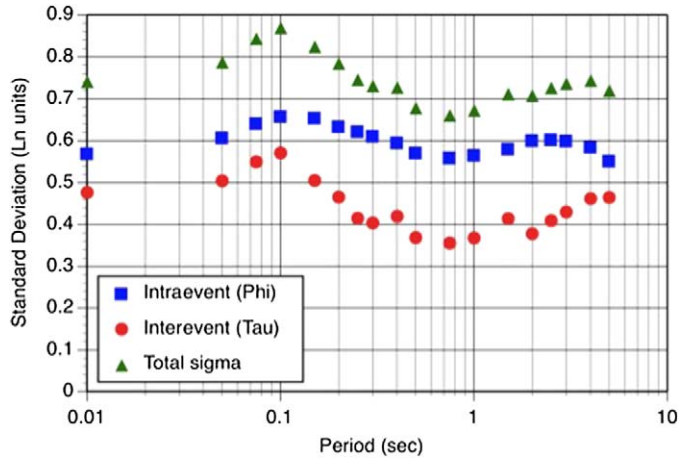

Figure 6. Regression results for interevent and intraevent terms and total sigma terms. Note: recommended values (see Table 3) are based on a smoothed value over all spectral periods.

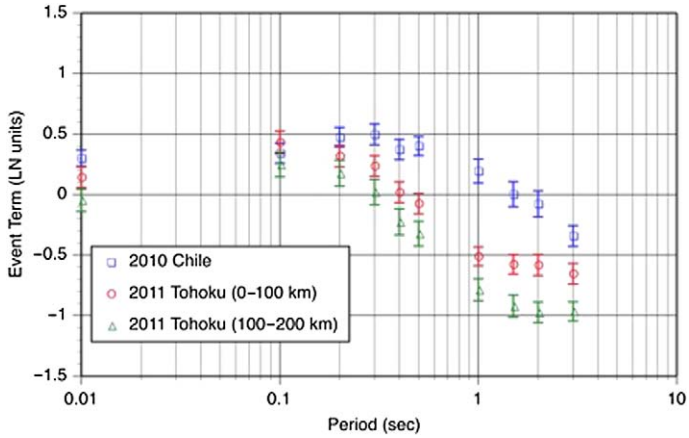

Figure 7. Event terms for the 2011 Tohoku, Japan, earthquake and the 2010 Maule, Chile, earthquake.

because the distance attenuation is similar to that in the model. For the Tohoku earthquake, the event terms are shown for two distance ranges: 0–100 km, and 100–200 km. The two earthquakes show a consistent pattern, with positive event terms at short periods and negative event terms at long periods. This indicates that the spectra shape of these and potentially future large megathrust events is richer in short-period content than that given by the model. To account for this bias in the model, the ΔC_1 terms for interface earthquakes are adjusted as shown in Table 4. Increasing the ΔC_1 at short periods leads to an increase in the short-period ground motions for large magnitudes. Similarly, decreasing ΔC_1 at long periods leads to a decrease in long-period ground motions for large magnitudes. The effect of change in the central ΔC_1 values is shown in Figure 8.

MAGNTIDUE SCALING FOR LARGE SLAB EARTHQUAKES

The break in large-magnitude scaling for slab events is not well constrained. An evaluation of magnitude scaling from slab events is shown in Figure 9. For reference, the magnitude

Table 4. Recommended period-dependent ΔC_1 Values for Interface earthquakes based on residual analysis of the Maule and Tohoku earthquakes with the GMPE model

Period (s)	Lower value[1]	Central value[1]	Upper value[1]
PGA	0.0	0.2	0.4
0.3	0.0	0.2	0.4
0.5	−0.1	0.1	0.3
1.0	−0.2	0.0	0.2
2.0	−0.3	−0.1	0.1
3.0–10.0	−0.4	−0.2	0.0

Note: Lower, central, and upper values are included to capture the model's epistemic uncertainty.
[1]For intermediate spectral periods, values should be interpolated based on log-spectral periods and linear values.

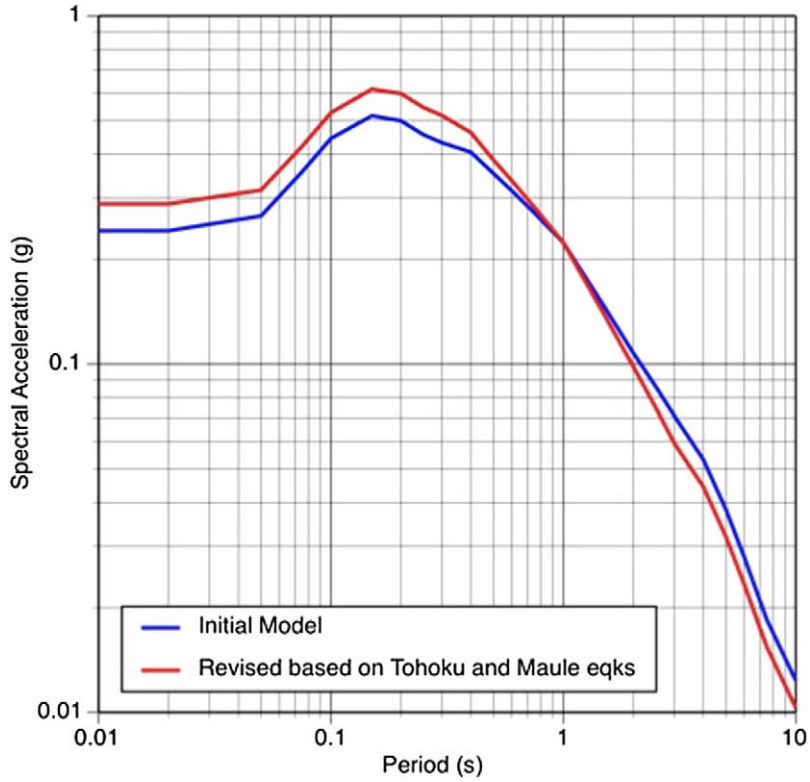

Figure 8. Effect of the recommended change (i.e., initial model versus revised model based on Tohoku and Maule earthquake data) in the ΔC_1 terms from Table 4.

scalings from Youngs et al. (1997) and the Zhao et al. (2006) are shown in relation to the magnitude scaling from the regression (solid red curve in color and gray curve in black and white). The data show that magnitude scaling is stronger than that in the Youngs et al. (1997) model in the **M**6.5–**M**7.5 range. Above **M**7.5, there are few data to constrain the model, but on average the data are below those from the regression model. A modification of ΔC_1 to center the break in the magnitude scaling at **M**7.5 (i.e., $C_1 = 7.8$ plus $\Delta C_1 = -0.3$) is shown by the dashed red curve. This value of $\Delta C_1 = -0.3$ is recommended for all spectral periods for slab events. To capture the epistemic uncertainty, an additional range of ΔC_1 of ± 0.2 is recommended in addition to the central value of $\Delta C_1 = -0.3$ (i.e., lower $\Delta C_1 = -0.5$, central $\Delta C_1 = -0.3$, and upper $\Delta C_1 = -0.1$) to capture the epistemic uncertainty in large-magnitude scaling for slab events.

EXAMPLES OF MEDIAN SPECTRA

Examples of the BC Hydro ground motion subduction model are shown for sites with a $V_{S30} = 760$ m/s located in the forearc region. Figure 10 shows the response spectra for interface earthquakes for **M**7.0, **M**8.0, and **M**9.0 earthquakes at rupture distances of 25, 50, 100, and 200 km. Figure 11 shows the response spectra for slab earthquakes at a hypocentral depth

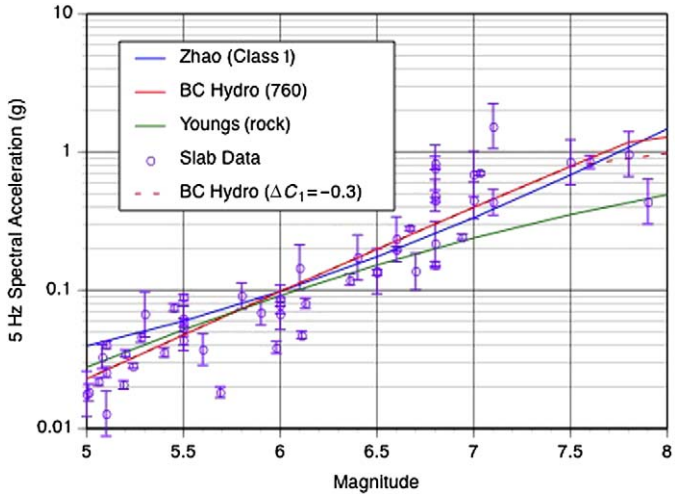

Figure 9. Evaluation of magnitude scaling for slab events. The data shown are the event terms adjusted to mean 5% spectral acceleration at a distance of 100 km.

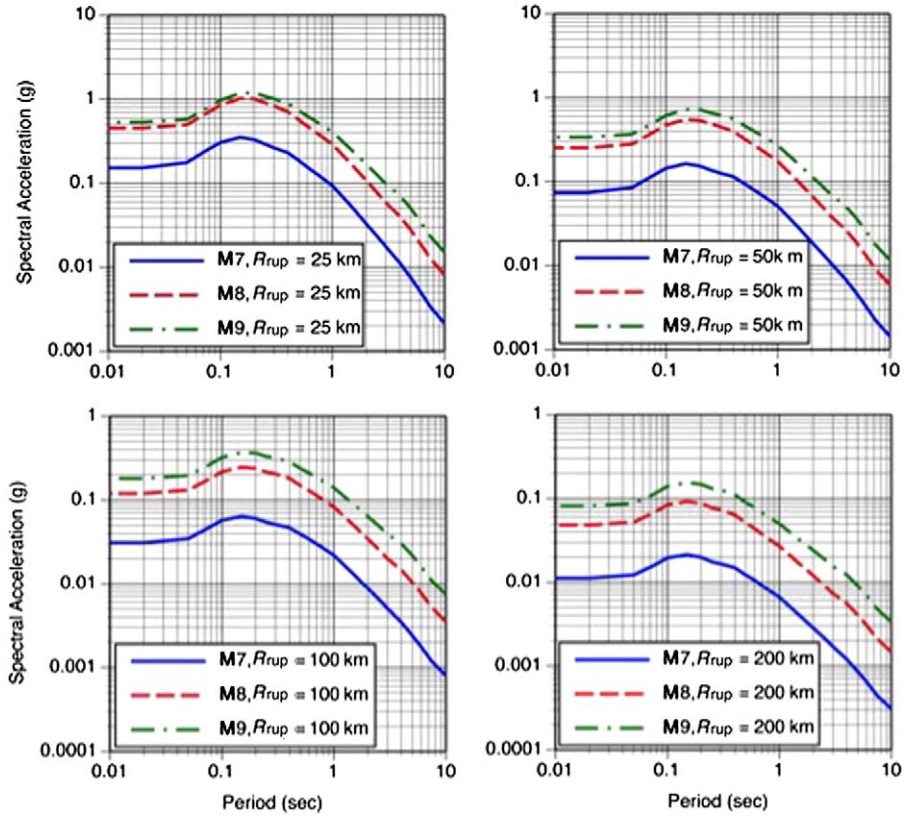

Figure 10. Examples of median spectra for interface earthquakes at sites with $V_{S30} = 760\,\mathrm{m/s}$ located in the forearc region.

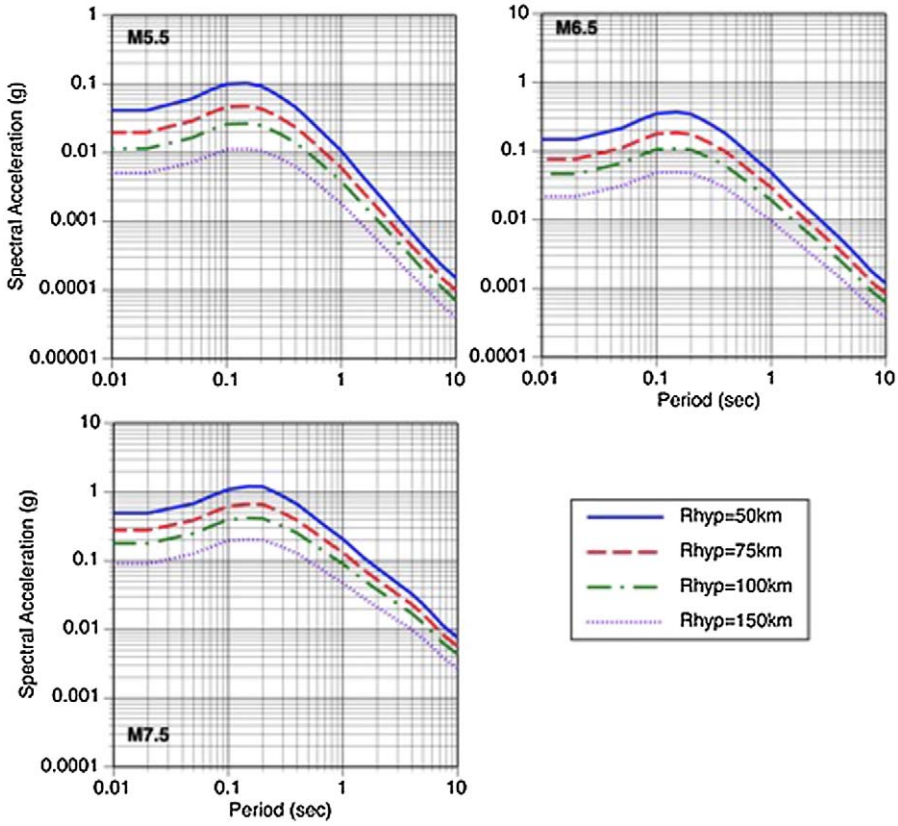

Figure 11. Examples of median spectra for slab earthquakes at a hypocentral depth of 50 km at sites with $V_{S30} = 760\,\mathrm{m/s}$ located in the forearc region.

of 50 km for **M**5.5, **M**6.5, and **M**7.5 earthquakes at hypocentral distances of 50 km, 75 km, 100 km, and 150 km.

EPISTEMIC UNCERTAINTY

The GMPE derived in this study is based on the combined data sets used in many of the current subduction GMPEs. This new global GMPE is intended to replace the older global GMPEs based on the larger data set used. To capture the epistemic uncertainty in the median ground motion, we developed a set of alternative scale factors for both the median and the alternative values of ΔC_1 as presented earlier.

The range of means of the region-specific event terms as determined by the regression analysis (BC Hydro 2012) are used to represent the epistemic uncertainty of the median scale factor. Figures 3a and 3b show that the median residuals in Japan, Mexico, and Taiwan range (i.e., the three regions that contribute the most number of recordings) approximately −0.2–0.2. Therefore, values of +0.2, 0.0, and −0.2 in natural log units are used to capture the epistemic uncertainty in the median at moderate magnitudes.

There is additional epistemic uncertainty in the median ground motion from large- magnitude earthquakes. As shown in Figure 2, the range of large- interface PGA values from the two sets of finite-fault simulations can be captured if the break in magnitude scaling is adjusted up and down by 0.5 magnitude units; however, part of this range is covered by the epistemic uncertainty (± 0.2) applied to the global model median as described previously. Combining the range in the median of ± 0.2 with a $\Delta C_1 \pm 0.2$ captures the range shown in Figure 2. Ultimately, these additional epistemic factors can be used to develop an applicable subduction GMPE logic tree for use in a PSHA study as performed for the BC Hydro (2012) study.

SUMMARY

This paper summarizes a larger and more detailed report (BC Hydro 2012) on the development of the subduction GMPE model. This newly developed model, which was used in the regional PSHA study (BC Hydro 2012) represents an advancement in subduction GMPE models if for no other reason than the inclusion of additional ground motion data with the previous data sets. Numerous comparisons between this new GMPE model and currently available GMPE models are contained in BC Hydro (2012). For distances less than approximately 100 km, the BC Hydro model predicts median ground motions that fall within the range of current GMPEs (note that the range in current subduction GMPE models is significantly larger than the range in crustal-model GMPEs). At larger distances, the BC Hydro model predicts lower ground motions based on the stronger attenuation, especially at backarc site locations. For intraslab events, the BC Hydro GMPE predicts ground motion values that are similar to the suite of currently available GMPE models over distances less than approximately 100 km and magnitudes less than approximately **M**7.0. For larger magnitudes and distances, the BC Hydro model tends to bound the range of GMPE model predictions for intraslab events.

The BC Hydro GMPE for subduction earthquakes is a global model. The epistemic uncertainties surrounding the constant term can be used to capture regional variations in average ground motion levels, but it does not capture changes in distance attenuation. The strengths of the new model are as follows: (1) it is based on a large global data set; (2) regional variations in the constant term are evaluated; and (3) the ΔC_1 term allows the user to adjust large- magnitude scaling without affecting smaller magnitudes. The weaknesses of the model are as follows: (1) it does not consider regional variations in V_{S30} scaling or the Q term, and (2) the forearc/backarc differences may be partly due to different linear distance scaling terms (θ_6) in Japan as compared to other regions.

ACKNOWLEDGMENTS

Funding for this work was provided by BC Hydro as part of the SSHAC Level 3 seismic hazard update for British Columbia, Canada. The development of the ground motion model benefited greatly from suggestions by workshop participants, including Brian Chiou, Robert Youngs, Gail Atkinson, Thomas Cheng, John Zhao, and Walter Silva. Data from the 2010 Maule, Chile, earthquake were provided by University of Chile Renadic; data from the 2012 Tohoku, Japan, earthquake were from the K-Net stations. We thank the three anonymous reviewers for their useful comments and suggestions that improved the manuscript.

APPENDIX

Please refer to the online version of this paper to access the supplemental tables and figures in the Appendix.

REFERENCES

Abrahamson, N. A., and Youngs, R. R., 1992. A stable algorithm for regression analyses using the random effects model, *Bulletin of Seismological Society of America* **82**, 505–510.

Abrahamson, N.A., Atkinson, G., Boore, D., Bozorgnia, Y., Campbell, K., Chiou, B., Idriss, I. M., Silva, W., and Youngs, R., 2008. Comparisons of the NGA ground-motion relations, *Earthquake Spectra* **24**(1), 45–66.

Abrahamson, N. A., and Silva, W. J., 2008. Summary of the Abrahamson and Silva NGA ground motion relations, *Earthquake Spectra* **24**, 67–98.

Atkinson, G. M., and Macias, G., 2009. Predicted ground motion for great interface earthquakes in the Cascadia subduction zone, *Bulletin of the Seismological Society of America* **99**, 1552–1578.

Atkinson, G. M., and Boore, D. M., 2003. Empirical ground-motion relationships for subduction-zone earthquakes and their application to Cascadia and other regions, *Bulletin of the Seismological Society of America* **93**, 1703–1729.

Atkinson, G. M., and Boore, D. M., 2008. Erratum to empirical ground-motion relationships for subduction-zone earthquakes and their application to Cascadia and other regions. *Bulletin of the Seismological Society of America* **98**, 2567–2569.

BC Hydro (2012). *Probabilistic Seismic Hazard Analysis (PSHA) Model*, vols. 1–4, *BC Hydro Engineering Report E658*,Vancouver.

Beyer, K., and Bommer, J. J., 2006. Relationships between median values and between aleatory variabilities for different definitions of the horizontal component of motion, *Bulletin of the Seismological Society of America* **96**, 1512–1522.

Boore, D. M., Watson-Lamprey, J., and Abrahamson, N. A., 2006. GMRotD and GMRotI: Orientation-independent measures of ground motion, *Bulletin of the Seismological Society of America* **96**, 1202–1511.

Boroschek, R., Contreras, V., Kwak, D. Y., and Stewart, J. P., 2012. Strong ground motion attributes of the 2010 M_w 8.8 Maule Chile, earthquake. *Earthquake Spectra* **28**(S1), S19–S38.

Campbell, K. W., and Bozorgnia, Y., 2008. NGA ground motion model for the geometric mean horizontal component of PGA, PGV, PGD, and 5% damped linear elastic response spectra for periods ranging from 0.01 to 10s, *Earthquake Spectra* **24**, 139–171.

Campbell, K. W., and Bozorgnia, Y., 2014. NGA-West2 ground motion model for the average horizontal components of PGA, PGV, and 5% damped linear acceleration response spectra, *Earthquake Spectra* **30**, 1087–1116.

Cheng, T., 2008. Processed strong ground motion data and metadata information for recordings from Taiwan, data submittal to BC Hydro, Vancouver.

Chiou, B., Darragh, R., Gregor, N., and Silva, W., 2008. NGA project database, *Earthquake Spectra* **24**, 23–44.

Crouse, C. B., 1991. Ground-motion attenuation equation for earthquake on Cascadia subduction-zone earthquake, *Earthquake Spectra* **7**, 210–236.

Crouse, C. B, Yogesh, K. V., and Schell, B. A., 1988. Ground motions from subduction zone earthquakes, *Bulletin of the Seismological Society of America* **78**, 1–25.

Douglas, J., 2010. Consistency of ground-motion prediction equations from the past four decades, *Bulletin of Earthquake Engineering* **8**, 1515–1526.

Garcia, D., Wald, D. J., and Hearne, M. G., 2012. A global earthquake discrimination scheme to optimize ground motion prediction equation selection, *Bulletin of Seismological Society of America* **102**, 185–203.

Gregor, N., Silva, W., Wong, I., and Youngs, R., 2002. Ground-motion attenuation relationships for Cascadia subduction zone megathrust earthquakes based on a stochastic finite-fault modeling, *Bulletin of Seismological Society of America* **92**, 1923–1932.

Ekström, G., Nettles, M., and Dziewoński, A. M., 2012. The global CMT project 2004–2010: Centroid-moment tensors for 13,017 earthquakes, *Physics of the Earth and Planetary Interiors* **200-201**, 1–9.

International Seismological Centre, 2014. Web page for the Bulletin of the International Seismic Centre, available at http://www.isc.ac.uk (last accessed 14 January 2016).

Lin, P.-S., and Lee, C.-T., 2008. Ground-motion attenuation relationships for subduction-zone earthquakes in Northeastern Taiwan, *Bulletin of the Seismological Society of America* **98**, 220–240.

Macias-Carrasco, M., 2008. Processed strong ground motion data and metadata information for recordings from Japan and Mexico, data submittal to BC Hydro.

Pacific Engineering, 2008. Processed strong ground motion data and metadata information for recordings from Central America, data submittal to BC Hydro.

Stewart, J. P., Midorikawa, S., Graves, R. W., Khodaverdi, K., Kishida, T., Miura, H., Bozorgnia, Y., and Campbell, K. W., 2013. Implications of the M_w9.0 Tohoku-Oki Earthquake for ground motion scaling with source, path, and site parameters, *Earthquake Spectra* **29**(S1), S1–S22.

Walling, M., Silva, W., and Abrahamson, N., 2008. Nonlinear site amplification factors for constraining the NGA models. *Earthquake Spectra* **24**, 243–255.

Youngs, R., Chiou, S., Silva, W., and Humphrey, J., 1997. Strong ground motion attenuation relationships for subduction zone earthquakes, *Seismic Research Letters* **68**, 58–73.

Zhao, J. X., Zhang, J., Asano, A., Ohno, Y., Oouchi, T., Takahashi, T., Ogawa, H., Irikura, K., Thio, H. K., Somerville, P. G., Fukushima, Y., and Fukushima, Y., 2006. Attenuation relations of strong ground motion in Japan using site classification based on predominant period, *Bulletin of the Seismological Society of America* **96**, 898–913.

Zhao, J. X., 2008. Processed strong ground motion data and metadata information for recordings from Japan, data submittal to BC Hydro, Vancouver.

(Received 3 October 2014; accepted 11 January 2015)